Am J Physiol Renal Physiol 293: F1209–F1213, 2007.
First published July 25, 2007; doi:10.1152/ajprenal.00097.2007.

Ficoll is not a rigid sphere

William H. Fissell,[1] Sargum Manley,[2] Anna Dubnisheva,[3] Jeffrey Glass,[4] Jeffrey Magistrelli,[3] Abigail N. Eldridge,[3] Aaron J. Fleischman,[3] Andrew L. Zydney,[5] and Shuvo Roy[3]

[1]*Departments of Nephrology and Hypertension and Biomedical Engineering; and* [3]*Department of Biomedical Engineering, The Cleveland Clinic, Cleveland, Ohio;* [2]*Department of Internal Medicine, University of Michigan, Ann Arbor, Michigan;* [4]*Department of Electrical and Computer Engineering, Duke University, Durham, North Carolina; and* [5]*Pennsylvania State University, University Park, Pennsylvania*

Submitted 26 February 2007; accepted in final form 28 June 2007

Fissell WH, Manley S, Dubnisheva A, Glass J, Magistrelli J, Eldridge AN, Fleischman AJ, Zydney AL, Roy S. Ficoll is not a rigid sphere. *Am J Physiol Renal Physiol* 293: F1209–F1213, 2007. First published July 25, 2007; doi:10.1152/ajprenal.00097.2007.—Polydisperse Ficoll mixtures have been used to explore glomerular sieving. Ficoll appears to be neither absorbed nor secreted by the renal tubule, and so urinary Ficoll concentrations reflect only the glomerular filtration barrier. The literature is contradictory regarding Ficoll's behavior as an idealized spherical solute. Further definition of Ficoll transport will inform interpretation of in vivo results. Flat-sheet membranes comprising a uniform array of slit pores measuring 8 nm by 45 μm were perfused with FITC-labeled Ficoll 70 and BSA. Ficoll and BSA concentrations were quantified by gel-permeation chromatography and Bradford assay, respectively. BSA and Ficoll molecules with diameters equal to approximately half of the slit pore width displayed hindered transport in agreement with modeled rigid sphere transport through slit-shaped pores. Ficoll molecules larger than ~0.65 slit width displayed transport rates in excess of predictions. Ficoll molecules with Stokes-Einstein diameters greater than the pore dimension were observed in permeate samples. We present data for Ficoll filtration through a novel array of well-defined pores, which illustrate that Ficoll is well modeled as an ideal sphere in one size domain, but the model breaks down as molecular diameter approaches pore size. These data inform the present debate regarding glomerular filtration and affect conclusions drawn from the use of Ficoll as a tracer molecule. The apparent hyperpermeability of Ficoll through slit-shaped pores suggests that further modeling incorporating deformation of the molecule is necessary when using Ficoll solutions to characterize membranes.

glomerulus; membrane; MEMS; micromachining; silicon

THE PHYSIOLOGICAL BASIS for glomerular permselectivity remains an area of active research in nephrology, and present theories do not fully explain all transport and histological observations (1, 6, 9–11, 14, 16, 17, 19, 20, 31–33, 36–39). In particular, the observed exponential decrease in solute concentrations from endothelial to epithelial sides of the glomerular basement membrane conflicts with the correlation between podocyte disruption and proteinuria (14, 16, 31, 33). A comprehensive model capturing the interactions between the endothelial glycocalyx, basement membrane, and podocyte slit diaphragm has remained elusive (35).

The kidney regulates excretion of biological solutes through multiple processes at different anatomic locations within the kidney. Any given solute might be degraded by the glomerular endothelium, filtered or rejected by the multilayered glomerular membrane, cleaved by enzymes bound to the brush border of proximal tubule cells, passively reabsorbed by paracellular solvent drag, or actively secreted or reabsorbed by tubule cells. The multitude of transport mechanisms within the kidney poses a challenge to exploration of glomerular function. Small solutes that are neither reabsorbed nor excreted by the tubule are valuable indicators of glomerular filtration rate.

Investigations of glomerular permselectivity have used a variety of tracer molecules to quantify glomerular solute transport, including natural and modified proteins, dextrans, and Ficoll. Ficoll, a branched copolymer of epichlorohydrin and sucrose, has been widely used as a test solute for filtration experiments, both in vivo and in vitro (2, 3, 7, 25, 27–29, 39). Ficoll has putative advantages over globular proteins in that it is uncharged and relatively inert, and over other polymers, such as dextran and polyethylene oxide (PEO), as viscosity evidence suggests it is more spherical than the linear, chain-like dextrans used in classic studies of glomerular permselectivity (3, 28). Deen et al. (3, 7, 8, 25) published extensive studies and reviews of transport of molecules through porous membranes. In these studies of solute diffusion and convection through a membrane with well-defined pores, track-etched membranes with monodisperse cylindrical pores were used to test diffusion of four polymers, poly(vinylpyrrolidone), poly(ethylene oxide), Ficoll 70, and Dextran T70. The track-etched membranes had pore diameters ranging from 30 to 70 nm, much larger than the test solutes. Transport data for Ficoll 70 matched predictions for uncharged spheres in cylindrical pores (7, 25).

Rippe and others (28, 39) deployed Ficoll extensively in their studies of glomerular filtration, and they estimated pore sizes and populations from Ficoll sieving data. However, in vivo data show significant differences between transport of Ficoll and globular proteins (1, 28, 32, 39). Ficoll, as well as dextran, sieving coefficients exceed those of globular proteins of similar molecular weight, an effect described as "hyperpermeability" of the polymers (39). It has been postulated that Ficoll has extensive conformational freedom in solution, in contrast to globular proteins, and consequently can pass more easily through narrow pores than could a rigid sphere (39). The possibility that Ficoll does not behave as a rigid sphere for convective transport through pores complicates pore size estimates based on Ficoll transport.

The discrepancy between the in vitro data obtained by Deen and colleagues, where Ficoll behaves as a nearly perfect sphere, and the in vivo data of Rippe, where Ficoll transport

Address for reprint requests and other correspondence: W. H. Fissell, Biomedical Engineering ND20, 9500 Euclid Ave, Cleveland, OH 44195 (e-mail: whf@alum.mit.edu).

The costs of publication of this article were defrayed in part by the payment of page charges. The article must therefore be hereby marked "*advertisement*" in accordance with 18 U.S.C. Section 1734 solely to indicate this fact.

differs from that of globular proteins, might be explained by the difference in pore sizes between the in vitro and in vivo experiments. Pores of the glomerular filtration barrier are estimated to have radii of ~4 nm, whereas the track-etched membranes deployed by Deen and colleagues are an order of magnitude larger. When expressed as the ratio of solute radius to pore radius, ($\lambda = r_s/r_p$), the difference between the two experimental models becomes more clear. Deen (3, 32) quantified transport of Ficoll and albumin for $0.1 < \lambda < 0.5$, whereas Rippe and colleagues explored Ficoll transport for $0.5 < \lambda < 1.3$.

A data set defining Ficoll transport through membranes with well-defined slit-shaped pores small enough to explore $0.5 < \lambda < 1.3$ would improve understanding of Ficoll's use as a tracer molecule in glomerular sieving experiments. To that end, a series of prototype membranes comprising sparse arrays of monodisperse slit-shaped pores were manufactured using silicon bulk and surface micromachining techniques (12, 13, 24). Convective transport of Ficoll 70 was quantified for 4-μm-thick silicon flat-sheet membranes comprising slit-shaped pores 8 nm × 45 μm.

MATERIALS AND METHODS

Fabrication of nanopore membranes. Nanopore membranes have been prototyped from silicon substrates by an innovative process based on microelectromechanical systems (MEMS) technology (12, 13, 24) (Fig. 1). The process uses the growth of a thin sacrificial SiO_2 (oxide) layer to define the critical submicron pore size of the filter. The oxide is etched away in the final step of the fabrication process to leave behind open pores. Thermal oxidation of silicon substrates can routinely provide oxides down to 5-nm thickness with <1% variation across a 100-mm-diameter wafer.

Surface modification. To limit membrane fouling by globular proteins, the silica surface was covalently modified with poly(ethylene glycol) (PEG) using the solution phase method of Larson et al. (30). This technique uses a single-step mechanism which covalently couples silicon surface silanol groups (Si-OH) to a PEG polymer through a trimethoxysilane group forming a Si-O-Si-PEG sequence by a methanol dehydration reaction. This method is appealing due to the ease of application and availability of commercial materials that can be used as received. It is a one-step procedure as opposed to other processes such as chemical vapor deposition or solution phase coupling that use a bridge molecule to form a covalent bond. For this reason, our group chose this deposition technique with slight modifications. The modifications included omitting all sonication steps and continuing the PEG deposition for 12 h.

Hydraulic permeability testing. Hydraulic permeability of silicon nanopore membranes was measured as described previously (12, 24). Briefly, membranes were mounted in a custom-built Ussing chamber and flushed with carbon dioxide to exclude nitrogen. The feed and permeate sides of the membrane were wetted with deionized water or PBS, and the feed side was continuously perfused at 0.5–1.0 ml/min by a roller pump. The outlet of the feed side was restricted by a clamp to generate hydrostatic pressures. Movement of the fluid-air meniscus within a calibrated syringe on the permeate side was timed and volumetric flows were calculated (Fig. 2).

Membrane permselectivity testing. Membrane arrays were examined under differential interference contrast light microscopy for defects. Measured hydraulic permeability to PBS of each defect-free membrane was used to calculate critical pore dimension h, as described by Deen and Davidson (7). The retentate side of the membrane was continuously perfused at a flow rate of 1 ml/min from a 100-ml reservoir of feed solution, and the permeate side of the membrane was wetted with 60 μl of PBS. Compressed air was used to generate a transmembrane pressure of 2 psi as monitored by a pressure transducer within the Ussing chamber (Entran, EPX 10PG, Les Clayes-sous-Bois, France). The ultrafiltration volume was monitored either in a calibrated syringe barrel (Hamilton, Reno, NV) capped with parafilm or in a length of microbore tubing immersed in saline. Membranes were perfused with 50 μg/ml polydisperse FITC-labeled Ficoll 70 (Sigma, St. Louis, MO) prepared after the method of Ohlson et al. (28). Permeate was collected at timed intervals at 2 psi driving pressure, corresponding to membrane fluxes of $\sim 10^{-8}$ m/s. Shear rates in the feed compartment were estimated to be 0.5 s at 1 ml/min feed flow rate. This corresponds to a mass transfer coefficient of $K_m = 1.0 \times 10^{-7}$ m/s as evaluated from the Leveque solution for

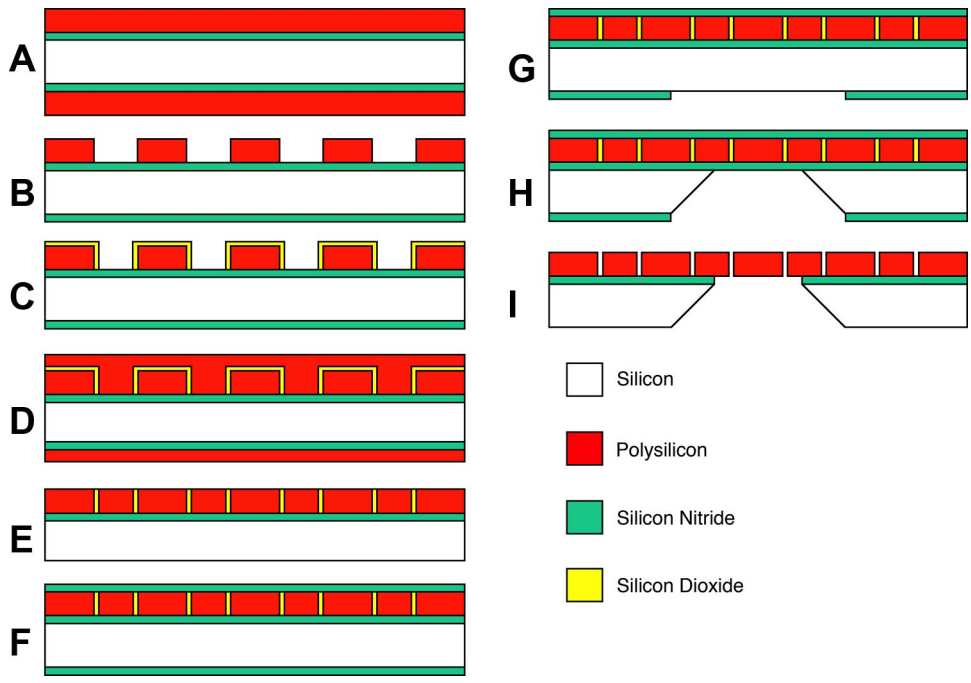

Fig. 1. Fabrication of silicon nanopore membranes (*A–I*) using microelectromechanical systems (MEMS) techniques depicted via wafer cross-sections (not to scale). The critical pore dimension (SiO_2 thickness in *C*) can be controlled between 5 and 50 nm with <1% variation across a 100-mm-diameter wafer.

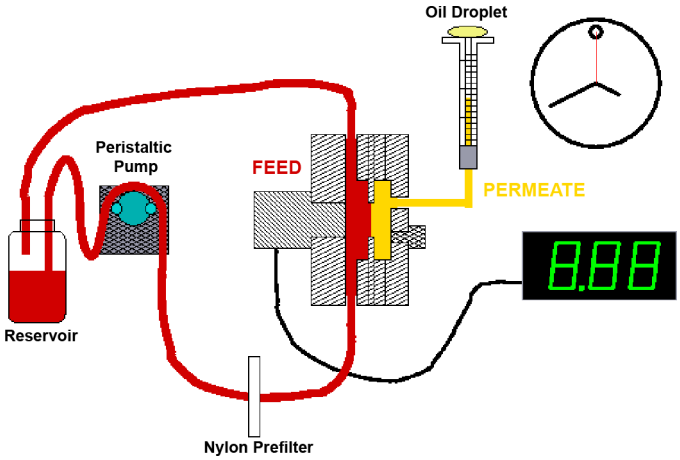

Fig. 2. Schematic of filtration cell. The membrane is sandwiched between a feed chamber and a permeate chamber. The feed solution is continuously circulated from a reservoir through the feed chamber by a peristaltic pump. The reservoir is pressurized with compressed air (not shown) and the pressure in the feed chamber is directly read by a pressure transducer. Permeate is accumulated, and volume is measured by displacement of a meniscus in a calibrated syringe. Flow rates are calculated by timing displacement of the meniscus.

fully developed channel flow for both the Ficoll 70 and BSA (42). Thus a reasonable estimate of concentration polarization effects is $C_w/C_b \sim 1.3$ for a fully retained solute where C_w is the solute concentration immediately adjacent to the membrane and C_b is the solute concentration in the bulk (feed) solution. Under the testing conditions, membrane Peclet number Pe_m, for bovine albumin is $\sim 10^1$, using Happel and Brenner's approximations for convective and diffusive hindrances, suggesting that convective transport dominates and our observed sieving coefficients reflect membrane rejection characteristics (42).

At the conclusion of each membrane test, the retentate side of the membrane was perfused with a dilute solution of 200 nm fluorescent polystyrene microspheres (#F8810, Molecular Probes, Willow Creek, OR) and 50–100 μl of permeate were collected. Serial dilutions of feed and permeate were examined by fluorescent microscopy for presence or absence of fluorescence signal.

Feed and permeate samples were analyzed by gel permeation chromatography with a Waters Ultrahydrogel 500 column on a Waters 600E system using a Waters 474 fluorescence detector. Size calibration of the column was performed with monodisperse Ficolls of known sizes, which were the kind gift of Dr. B. Rippe, Lund University (Lund, Sweden). Membranes were perfused with BSA (Fraction V, Sigma) at a concentration of 4 g/l in 150 mM PBS in a similar manner. Albumin (BSA) feed and permeate samples were analyzed by Bradford assay (Bio-Rad, Hercules, CA). Sieving coefficients were calculated as the ratio of concentration in the permeate to the concentration in the feed solution.

Statistics. Experiments were repeated in triplicate and protein assays in duplicate. Means and SE were calculated using Microsoft Excel for Macintosh.

RESULTS

Prototype silicon nanoporous membranes were manufactured with highly uniform, smooth walled, slit-shaped pores (Fig. 3). Pore size could be controlled within 1 nm over a size range from 8 to 90 nm (24). Sample membranes randomly selected from each wafer were analyzed by scanning electron microscopy, and pore sizes were measured. Pore size was highly uniform, varying by <1% across samples from entire

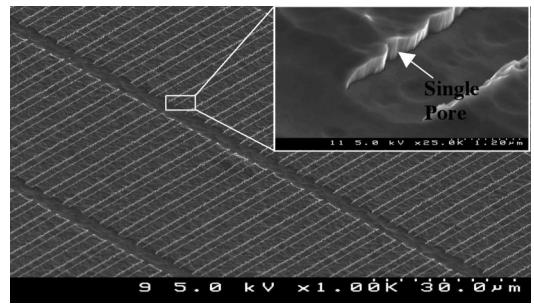

Fig. 3. Silicon nanopore membrane. Scanning electron micrograph of a silicon nanopore membrane. The membrane is fabricated as a thin film on a flat substrate. The pores are arranged in regular rows. Each pore is 8 nm in critical dimension, and 45 μm in long dimension, and penetrates down into the plane of the membrane sheet (arrow, *inset*).

100-mm wafer. Gas transport of carbon dioxide, nitrogen, and argon was consistent with transition regime and Knudsen flow, confirming pore size (12). Liquid flow of water and PBS each closely matched calculated Poiseuille flow over a range of critical pore sizes from 9 to 90 nm as measured by scanning electron microscopy (SEM; Fig. 4). The Poiseuille equation was then used to obtain the critical pore dimension (h) for membranes used for permselectivity testing, and not directly examined by SEM

$$h = \left(\frac{12\eta L Q}{w N_p \Delta P}\right)^{\frac{1}{3}}$$

where w is the slit pore width, L is the membrane thickness, η is viscosity, N_p is the number of pores, Q is volumetric flow, and ΔP is transmembrane pressure.

PEG-modified membranes displayed size-dependent rejection of Ficolls (Fig. 5). When sieving coefficient was plotted as a function of λ, the ratio of molecule diameter to pore dimension (analogous to $\lambda = r_s/r_p$ for cylindrical pores), convective transport of Ficoll exceeded that predicted for a rigid spherical solute in a slit-shaped pore for $\lambda > 0.6$. Convective transport of Ficoll molecules with predicted Stokes-Einstein radius larger than the nominal membrane pore size ($\lambda > 1.0$) was observed. The observed albumin sieving coefficient for the

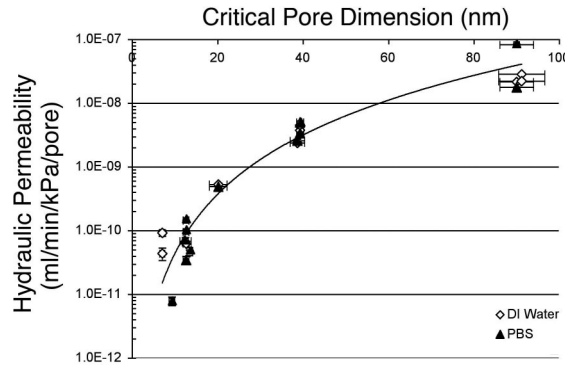

Fig. 4. Hydraulic permeability of silicon nanopore membranes. Hydraulic permeability (*y*-axis) of deionized water (◇) and PBS (▲) for silicon nanopore membranes with pore height 8–90 nm is plotted as a function of pore height (*x*-axis). Observed hydraulic permeability for both liquids was as predicted by Poiseuille flow through a slit pore (solid line).

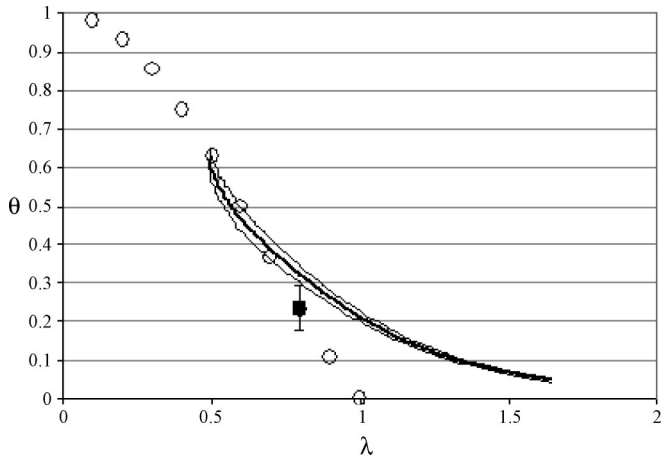

Fig. 5. Observed transport of BSA, Ficoll 70, and predicted transport of rigid spherical molecules through a slit pore. Observed sieving coefficients θ (*y*-axis) for BSA (■) and Ficoll 70 (mean, solid line, with thin lines above and below denoting means ± SE) are plotted against λ, the ratio of molecular radius to pore half-width. Predicted sieving coefficients for rigid spheres in a slit pore (○) from numerical solutions after Happel and Brenner (32) are plotted against λ. The observed sieving coefficient for a globular protein, albumin, closely matches the numerical solution. Ficoll 70 transport matches predicted values for molecules with λ = 0.5–0.6 but exceeds models for a rigid sphere as molecular size approaches pore size.

PEG-modified membrane was measured at 0.24 ± 0.058 (Fig. 5).

DISCUSSION

Polydisperse Ficoll has been extensively used as an inert test solute for examination of glomerular transport in laboratory animals and as a probe for exploring diffusion through porous media (1, 9–11). In vivo, observed sieving coefficients for Ficoll exceed those for neutral globular proteins of similar molecular radius, leading to speculation that Ficoll may not behave as an ideal rigid sphere under in vivo transport conditions (39). In contrast, experiments with track-etched membranes having uniform cylindrical pores yielded data well fit by a spherical model (3, 7, 25). However, previous studies of Ficoll in track-etched membranes did not explore limiting cases where the size of the Ficoll molecule approached or surpassed the pore dimension (3, 8, 25). The present report extends the experimental data regarding convective Ficoll transport through well-defined slit-shaped pores with critical dimension approximately equal to the Stokes-Einstein diameter of the solutes tested. This is the reverse of the usual experimental situation, where the Ficoll molecule is used to characterize the pores in the membrane. The data suggest that for Ficoll molecules less than half the critical pore dimension, the model of a spherical molecule predicts convective transport accurately, but as λ approaches unity, rejection is lower than expected for a rigid sphere, suggesting polymer deformation or that the molecule is not spherical, and the deviation from the spherical is only noticeable in tightly fitting, well-defined pores. Further experiments measuring sieving coefficients over a range of membrane fluxes and thus shear rates will help to define this more rigorously. Polymer confinement has been extensively studied from theoretical and experimental approaches, including linear molecules, such as polystyrene and DNA, as well as branched molecules (4, 5, 15, 21, 23, 26, 40, 41). Polymer transport into porous media has been modeled by the stretching of a coiled molecule due to the elongational flows and shear forces in a pore or its entry region. Interestingly, shear rates in our experiment are three orders of magnitude smaller than those reported for shear-dependent deformation of linear polymers (23). The physics of polymer deformation is related to the Deborah number, De, the product of the shear rate and characteristic molecular relaxation time. For large shears or long relaxation times, corresponding to De $>>$ 1, the polymer undergoes an affine deformation and aligns with fluid streamlines. For our system, the shear rates inside the pore are $\sim 10^4$ s; thus Ficoll elongation would only be expected if the characteristic relaxation time is on the order of $1/\gamma = 10^{-4}$ s. This is much longer than typical relaxation times reported in the literature for other polymers of similar size to the Ficoll examined in this work.

How, then, might we explain our results? Concentration polarization and concentration-dependent increases in viscosity are unlikely to explain the multiple order-of-magnitude difference between our observations and the predicted shear rates needed for polymer deformation, as solvent viscosity alone was adequate to predict pressure-driven flow through the membrane for dilute Ficoll and albumin solutions. Insight into our results is gained by comparing the theory and experiments in the literature with the experiments described here.

Our experimental apparatus is quite different from other published analyses both in the molecule analyzed and the pore structures deployed. The experiments of Neel, Anderson, and Zydney (4, 21, 23, 26, 40, 41) all consider linear molecules in cylindrical pores, as do the analyses of Wall and de Gennes. These represent transitions from highly entropic states with many degrees of freedom, that is, a dilute polymer in bulk solution, to a very highly ordered structure, the polymer approximating a straight line. In the limiting case, the polymer is completely confined, with the only remaining degrees of freedom being its axial rotation and its linear position in the pore. de Gennes' analysis of branched polymers shares this model. These represent nearly "worst case" scenarios for the forces and energies needed to compel polymer entry into the pore. Our experiment tests a very different paradigm, a branched molecule in a slit-shaped pore. This confines the polymer in one dimension only, allowing the molecule to retain multiple degrees of freedom within the pore. This physical situation was considered qualitatively by Brooks and Cates (5), which considered the change in entropy as an unconfined chain is progressively constrained into a pancake-like morphology. The significantly higher entropy of this two-dimensional (2-D) confinement compared with that in a cylindrical pore was experimentally confirmed by Craighead et al. (18), who observed spontaneous ejection of DNA strands from a region of 3-D confinement to an area of 2-D confinement. Our observation that Ficoll transmission may be shear dependent even at low shear forces suggests that further analysis of this phenomenon is necessary to understand the behavior of Ficoll in pores that are similar in size to the Stokes-Einstein diameter of the Ficoll.

For BSA, an anionic globular protein, the sieving coefficient was nearly exactly the value predicted by the Happel and Brenner approximation for a rigid perfect sphere in a slit pore (0.24 ± 0.06 vs. 0.239). At physiological pH, the poly(ethylene glycol) layer on the pore surface is expected to be completely

uncharged. Thus electrostatic hindrance is not expected and, despite albumin's negative charge ($Z \sim -18$), steric and hydrodynamic effects are expected to dominate. If the pore surface were charged, the Debye length at physiological tonicity is estimated to be $\sim$1 nm, the same order of magnitude as the pore size and the albumin radius. Numerical solutions to the linearized Poisson-Boltzmann equation for an anionic tracer molecule with net charge -18 in an 8-nm silica pore slit pore at physiological pH suggest electrostatic hindrances $\sim 10^{-1}$, similar to those from excluded volume and hydrodynamic effects (Hasselbrink EF, personal communication). Although we cannot exclude an electrostatic component to the observed sieving coefficient for albumin, the agreement with purely steric prediction is striking.

The observation that Ficoll appears considerably deformable in solution at physiological tonicity and moderate shear rates influences interpretation of in vivo studies examining transport of neutral and charged Ficoll and may help explain observed discrepancies between Ficoll and globular proteins (1, 17). More quantitative modeling of polymer confinement in planar geometries will be of great help in guiding interpretation of future experimental data.

REFERENCES

1. **Asgeirsson D, Venturoli D, Rippe B, Rippe C.** Increased glomerular permeability to negatively charged Ficoll relative to neutral Ficoll in rats. *Am J Physiol Renal Physiol* 291: F1083–F1089, 2006.
2. **Bohrer MP, Deen WM, Robertson CR, Troy JL, Brenner BM.** Influence of molecular configuration on the passage of macromolecules across the glomerular capillary wall. *J Gen Physiol* 74: 583–593, 1979.
3. **Bohrer MP, Patterson GD, Carroll PJ.** Hindered diffusion of dextran and Ficoll in microporous membranes. *Macromolecules* 17: 1170–1173, 1984.
4. **Brochard F, de Gennes PG.** Dynamics of confined polymer chains. *J Chem Physics* 67: 52–56, 1977.
5. **Brooks JT, Cates ME.** The role of added polymer in dilute lamellar surfactant phases. *J Chem Physics* 99: 5467–5480, 1993.
6. **Comper WD.** Charge selectively is a concept that has yet to be demonstrated. *Am J Physiol Renal Physiol* 281: F992–F993, 2001.
7. **Davidson MG, Deen WM.** Hindered diffusion of water-soluble macromolecules in membranes. *Macromolecules* 21: 3474–3481, 1988.
8. **Deen WM.** Hindered transport of large molecules in liquid-filled pores. *AIChE J* 33: 1409–1425, 1987.
9. **Deen WM, Lazzara MJ.** Glomerular filtration of albumin: how small is the sieving coefficient? *Kidney Int Suppl* 44: S63–S64, 2004.
10. **Deen WM, Lazzara MJ, Myers BD.** Structural determinants of glomerular permeability. *Am J Physiol Renal Physiol* 281: F579–F596, 2001.
11. **Deen WM.** What determines glomerular capillary permeability. *J Clin Invest* 114: 1412–1414, 2004.
12. **Fissell WH, Humes HD, Roy S, Fleischman A.** Initial characterization of a nanoengineered ultrafiltration membrane. *J Am Soc Nephrol* 13: 602A, 2002.
13. **Fissell WH, Manley S, Westover A, Humes HD, Fleischman AJ, Roy S.** Differentiated growth of human renal tubule cells on thin-film and nanostructured materials. *ASAIO J* 52: 221–227, 2006.
14. **Fujigaki Y, Nagase M, Kobayasi S, Hidaka S, Shimomura M, Hishida A.** Intra-GBM site of the functional filtration barrier for endogenous proteins in rats. *Kidney Int* 43: 567–574, 1993.
15. **Gay C, de Gennes PG, Raphaël E, Brochard-Wyart F.** Injection threshold for a statistically branched polymer inside a nanopore. *Macromolecules* 29: 8379–8382, 1996.
16. **Ghitescu L, Desjardins M, Bendayan M.** Immunocytochemical study of glomerular permeability to anionic, neutral and cationic albumins. *Kidney Int* 42: 25–32, 1992.
17. **Guimaraes MA, Nikolovski J, Pratt LM, Greive K, Comper WD.** Anomalous fractional clearance of negatively charged Ficoll relative to uncharged Ficoll. *Am J Physiol Renal Physiol* 285: F1118–F1124, 2003.
18. **Han J, Turner SW, Craighead HG.** Entropic trapping and escape of long DNA molecules at submicron size constriction. *Phys Rev Lett* 83: 1688–1691, 1999.
19. **Hilliard LM, Osicka TM, Clavant SP, Robinson PJ, Nikolic-Paterson DJ, Comper WD.** Characterization of the urinary albumin degradation pathway in the isolated perfused rat kidney. *J Lab Clin Med* 147: 36–44, 2006.
20. **Koltun M, Comper WD.** Retention of albumin in the circulation is governed by saturable renal cell-mediated processes. *Microcirculation* 11: 351–360, 2004.
21. **Latulippe DR, Ager K, Zydney AL.** Flux-dependent transmission of supercoiled plasmid DNA through ultrafiltration membranes. *J Membrane Sci* 294: 169–177, 2007.
22. **Lavrenko PN, Mikriukova OI, Okatova OV.** On the separation ability of various ficoll gradient solutions in Zonal centrifugation. *Anal Biochem* 166: 287–297, 1987.
23. **Long TD, Anderson JL.** Flow-dependent rejection of polystyrene from microporous membranes. *J Polymer Sci Polymer Physics Ed* 22: 1261–1281, 1984.
24. **Magistrelli JM.** *Investigating fluid flow through silicon nanoporous membranes (Master's thesis).* Cleveland, OH: Department of Chemical Engineering, Case Western Reserve Univ., 2004.
25. **Mitchell BD, Deen WM.** Effect of concentration on the rejection coefficients of rigid molecules in track-etch membranes. *J Colloid Interface Sci* 113: 132–142, 1986.
26. **Nguyen QT, Neel J.** Characterization of ultrafiltration membranes. IV. Influence of the deformation of macromolecular solutes on the transport through ultrafiltration membranes. *J Membrane Sci* 14: 111–128, 1983.
27. **Ohlson M, Sörensson J, Lindström K, Blom AM, Fries E, Haraldsson B.** Effects of filtration rate on the glomerular barrier and clearance for four differently shaped molecules. *Am J Physiol Renal Physiol* 281: F103–F113, 2001.
28. **Ohlsson M, Sörensson J, Haraldsson B.** Glomerular size and charge selectivity in the rat as revealed by FITC-Ficoll and albumin. *Am J Physiol Renal Physiol* 279: F84–F91, 2000.
29. **Oliver JD, Anderson S, Troy JL, Brenner BM, Deen WM.** Determination of glomerular size selectivity in the normal rat with Ficoll. *J Am Soc Nephrol* 3: 214–228, 1992.
30. **Papra A, Gadegaard N, Larson NB.** Characterization of ultrathin poly(ethylene glycol) monolayers on silicon substrates. *Langmuir* 17: 1457–1460, 2001.
31. **Pavenstadt H, Kriz W, Kretzler M.** Cell biology of the glomerular podocyte. *Physiol Rev* 83: 253–307, 2003.
32. **Rippe C, Asgeirsson D, Venturoli D, Rippe A, Rippe B.** Effects of glomerular filtration rate on Ficoll sieving coefficients (theta) in rats. *Kidney Int* 69: 1326–1332, 2006.
33. **Ryan GB, Karnovsky MJ.** Distribution of endogenous albumin in the rat glomerulus: role of hemodynamic factors in glomerular barrier function. *Kidney Int* 9: 36–45, 1976.
34. **Ryman-Rasmussen JP, Riviere JE, Monteiro-Riviere NA.** Penetration of intact skin by quantum dots with diverse physicochemical properties. *Toxicol Sci* 91: 159–165, 2006.
35. **Smithies O.** Why the kidney glomerulus does not clog: a gel permeation/diffusion hypothesis of renal function. *Proc Natl Acad Sci USA* 100: 4108–4113, 2003.
36. **Somers D.** Diagenic barriers-the glomerular barrier to albumin diffusion in the afferent glomerular capillary is created by fluid flow: a mathematical model. *J Am Soc Nephrol* 16: 440A, 2005.
37. **Somers D.** On the nature of the glomerular barrier to albuminuria: electrokinetic glomerulus theory. *J Am Soc Nephrol* 6: 109, 2005.
38. **Somers D.** Diagenic membrane barriers and the function of the slit diaphragm. *J Am Soc Nephrol* 16: 441A, 2005.
39. **Venturoli D, Rippe B.** Ficoll and dextran vs. globular proteins as probes for testing glomerular permselectivity: effects of molecular size, shape, charge, and deformability. *Am J Physiol Renal Physiol* 288: F605–F613, 2005.
40. **Wall FT, Chin JC.** Configurations of macromolecular chains confined to strips or tubes. *J Chem Physics* 66: 3066–3069, 1977.
41. **Wall FT, Mandel F, Chin JC.** Self-avoiding random walks subject to external spatial constraints. *J Chem Physics* 65: 2231–2234, 1976.
42. **Zydney AL, Zeman LJ.** *Microfiltration and Ultrafiltration.* New York: Marcel Dekker, 1996.